SPATIAL DISTRIBUTION AND ITS SEASONALITY OF SATELLITE-DERIVED VEGETATION INDEX (NDVI) AND CLIMATE IN SIBERIA

RIKIE SUZUKI[a,*], TOMOYUKI NOMAKI[b] and TETSUZO YASUNARI[a,c]

[a] *IGCR-Tsukuba, Frontier Research System for Global Change (FRSGC), Tsukuba, Japan*
[b] *Data Analysis and Research Division, Remote Sensing Technology Center of Japan (RESTEC), Tokyo, Japan*
[c] *Institute of Geoscience, University of Tsukuba, Tsukuba, Japan*

ABSTRACT

The Normalized Difference Vegetation Index (NDVI) distribution and its seasonal cycle were investigated in relation to temperature and precipitation over Siberia and its surrounding regions. The analyses used 5-year (1987–1991) monthly means. The monthly mean NDVI was calculated from the third-generation monthly Global Vegetation Index (GVI) product; monthly temperature and precipitation at 611 stations were calculated from Global Daily Summary (GDS) data.

The 611 stations were classified by cluster analysis into 10 classes based on the NDVI seasonal cycle (March–October). The geographical distribution characteristics of the NDVI cycle were described using temperature, precipitation and Olson's land-cover type. In northern regions, where tundra vegetation prevails and temperatures and precipitation are low, the amplitude of the NDVI seasonal cycle is small. In southern regions, where temperatures are high and there is little precipitation, the seasonal amplitude of the NDVI is small because of the arid land type. Forested regions were split into six classes, each characterized by large amplitudes in the NDVI seasonal cycle. The phenological characteristics of the forest classes were noted. For example, a forest-class localized near Lake Baikal shows higher NDVI values, even with the presence of snow cover in March, compared with other regions. This high NDVI value suggests that the exposed green canopy of the coniferous forest can be observed even when snow is present. In addition, the NDVI peaks at stations near 60°N, where the maximum monthly temperature is around 18°C. This result suggests that the optimum temperature-precipitation environment coincides to the area in Siberia where the maximum monthly temperature is 18°C. Copyright © 2001 Royal Meteorological Society.

KEY WORDS: cluster analysis; ecosystem; GVI; phenology; precipitation; Siberia; taiga; temperature; tundra

1. INTRODUCTION

Differences in the Earth's vegetation cover are strongly controlled by the climate of each region, as noted in, for example, Walter (1973) and Woodward (1987). In addition, the phenological features of vegetation are closely linked to climatological seasonal cycles. Generally, in mid and high latitudes, plants start foliation in response to the rise in temperature from spring to summer, and subsequently evolve to senescence and then to dormancy as temperatures fall in autumn and winter. Vegetation in dry regions does not show a marked seasonal cycle, nor does the leaf mass of the canopy of evergreen forests clearly change with the seasons.

Since the 1980s, global vegetation data have been measured from space by satellite-borne instruments. Much satellite-derived information on global vegetation is now available for climatological and plant-geographical studies over large regions.

---

* Correspondence to: IGCR-Tsukuba, Frontier Research System for Global Change (FRSGC), c/o National Research Institute for Earth Science and Disaster Prevention, Tsukuba 305-0006, Japan; e-mail: rikie@bosai.go.jp

1.1. Normalized Difference Vegetation Index (NDVI)

The difference in the reflectance of chlorophyll pigment between the visible and near-infrared parts of the spectrum provides a means for monitoring the density and vigour of green vegetation (e.g. Tarpley *et al.*, 1984). The National Oceanic and Atmospheric Administration (NOAA) satellite has a five-channel radiometer, Advanced Very High Resolution Radiometer (AVHRR), with channel 1 in visible (0.58–0.68 μm) and channel 2 in near-infrared (0.73–1.10 μm) spectral bands. The Normalized Difference Vegetation Index (NDVI), a well-known vegetation index, is computed as $NDVI = (Ch2 - Ch1)/(Ch2 + Ch1)$, where Ch1 and Ch2 are the surface reflectance from AVHRR channels 1 and 2, respectively (e.g. Tarpley *et al.*, 1984). Arithmetically, NDVI ranges from -1.0 to 1.0, but actual values at the Earth's surface range from -0.1 to 0.7. The remotely sensed value of the NDVI allows the 'greenness' of vegetation to be analysed at regional to global scales. NDVI data provide spatially continuous, long-term information on vegetation, and thus are useful for studying seasonal vegetation cycles (e.g. Gutman, 1999).

1.2. Background and purpose of the study

This study focuses on climate-vegetation seasonality, and its regional characteristics over Siberia and its surrounding areas as revealed by the NDVI. Siberia was chosen because of the remarkable long-term rise in temperatures found there (especially in winter) in global warming studies (IPCC, 1996). A long-term change in snow depth was also noted by Ye *et al.* (1998). An increase in the values in a decade-long (1981–1991) NDVI time series was found over high latitudes in the Northern Hemisphere (Myneni *et al.*, 1997, 1998). Furthermore, the thick taiga vegetation over such an extensive area has great potential to provide water vapour to the atmosphere through evapotranspiration (e.g. Suzuki *et al.*, 1998). The vegetation data should give proxy information on transpiration from the ground so that this study will improve understanding of the water cycle over an extensive area.

Part of the GEWEX Asian Monsoon Experiment (GAME), an international project under the Global Energy and Water Cycle Experiment (GEWEX), GAME–Siberia is being implemented in the Lena river basin, and focuses on energy and water cycle processes (GAME–International Science Panel, 1998). Results from the present study will add to knowledge of hydro-meteorological sciences over Siberia and the region's impact on the global climate system.

NDVI data have been used in the past to interpret the seasonal cycle in the phenological characteristics of global vegetation. For example, Moulin *et al.* (1997) described the phenological evolution (dormancy, growth and senescence) of global vegetation by analysing seasonal variations in the NDVI. Furthermore, global vegetation cover has been classified using NDVI-derived phenological characteristics of vegetation (e.g. Norwine and Greegor, 1983; DeFries and Townshend, 1994). However, global-scale studies provide only limited information on Siberia. No previous study has closely examined the phenology of Siberian vegetation using NDVI data.

This study complements the study by Suzuki *et al.* (2000), which revealed a close relationship between NDVI distribution and temperature and precipitation distributions along meridional (north–south) transects in Siberia. This study focuses on the vegetation phenology that can be inferred from the NDVI time series, and how spatial variation in the phenology relates to temperature and precipitation over Siberia and adjacent areas. The results of this study will improve understanding of the climatological implications of seasonal change in Siberian vegetation.

2. DATA AND ANALYSES

The study analyses monthly mean values of NDVI, temperature and precipitation. The mean values are 5-year averages from 1987 through to 1991. The region analysed is from 40° to 160°E, and from 40° to 75°N, as shown in Plate 1. This region covers Siberia, and includes European Russia, Mongolia and part of China.

2.1. Temperature and precipitation

Surface air temperature and precipitation data were obtained from the CD-ROM 'Global Daily Summary (GDS)' from the National Climate Data Center (NCDC) of the NOAA (NOAA National Climate Data Center, 1994). The GDS includes daily maximum/minimum temperatures, daily precipitation and 3-hourly weather at 10 277 surface World Meteorological Organization (WMO) stations around the world.

There are more than 1200 GDS stations in the region analysed. Station distribution, however, is non-uniform; there are many stations in southern Russia and northern China, but few in northern Siberia. As mentioned in the next section, the NDVI at each GDS station is calculated by averaging all NDVI pixels in a $1° \times 1°$ latitude–longitude box around each station. Some stations, mainly in southern Russia and China, were excluded from the analysis to prevent overlapping among boxes because of the dense station distribution. Consequently, 611 stations were used for the analysis, as indicated in Plate 1. This elimination process helped to prevent crowding in the plotting point distributions in Plate 3 and Figures 3 and 8 caused by non-uniform station distribution.

The monthly mean temperature for the 5 years at the 611 stations was calculated from the daily temperature $(T_{d_{max}} + T_{d_{min}})/2$, where $T_{d_{max}}$ and $T_{d_{min}}$ are the daily maximum and minimum temperatures, respectively (daily mean temperature is not available in the GDS). Monthly precipitation was calculated at these 611 stations by summing the daily precipitation value in the GDS dataset. The monthly precipitation unit is normalized to 'mm/30 days' even for months not containing 30 days.

2.2. Third-generation global NDVI data

The original 4-km resolution Global Area Coverage (GAC) AVHRR data were re-sampled to a coarser resolution, and the weekly Global Vegetation Index (GVI) product, which uses $0.144° \times 0.144°$ map pixels (so-called GVI map pixel; 16×16 km resolution at the equator), was developed (e.g. Tarpley, 1991). The second generation GVI datasets constructed by this process (e.g. Kidwell, 1997) have been used in many studies.

The third-generation C-level NDVI data (NOAA National Climate Data Center, 1998) used in this study are a monthly NDVI dataset developed from the second generation GVI. The third-generation NDVI data result from reprocessing weekly second generation GVI datasets (Gutman et al., 1995). Channel 1 and 2 AVHRR reflectances were re-calibrated (Rao and Chen, 1995, 1996) to account for sensor degradation and satellite orbital drift, and then cloud-contaminated pixels were screened. The spatial resolution is the same as in the second generation GVI.

The monthly processing flow from weekly products follows this path: (i) quality/cloud flags were applied on a weekly basis, which caused data gaps; (ii) the NDVI was averaged over 1 month (five weekly composites) for each map cell to reduce both the data gaps and some of the angular variability (some weeks were included in both the current and previous months); (iii) persistently cloudy regions, which would result in a data void in the monthly averaged images, were filled using bilinear spatial interpolation; (iv) 3×3 map cell running average smoothing was performed to compensate for the imperfect cloud screening, to filter out atmospheric and angular variability, and to compensate both for varying numbers of observations used in computing monthly averages and for discontinuities in the random spatial sampling of the original GAC AVHRR data into the GVI map pixels.

The third-generation C-level NDVI data product may yet contain small errors related to latitudinal differences in the Sun–Earth–satellite geometry, or to the process of making the GVI from the high resolution GAC dataset (e.g. as summarized by Goward et al., 1993). We assume that any unfavourable biases or errors in the data product are small for this study, which targets the seasonal cycle of the NDVI over Siberia and the surrounding area in a limited latitudinal zone.

The monthly NDVIs at all GVI map pixels in any $1° \times 1°$ box (8×8 pixels) that had a GDS station close to its centre were averaged. Using this average value as a mean for each box, we computed 5-year monthly mean NDVIs for each GDS station. The NDVI values in November–February were not used for this statistic, because the NDVI in those months can contain meaningless values linked to low sun angles

(e.g. Justice *et al.*, 1985). In addition, the CD-ROM dataset for March 1989 and March 1990 contains some unrealistically large values; these 2 months were therefore excluded from the statistics.

2.3. Land-cover classification data

Olson's CD-ROM 'Olson World Ecosystems' (Olson, 1992) was used to classify land cover. This land-cover data details the global distribution of 59 different land-cover classes on a $10' \times 10'$ grid. To obtain a more general land-cover classification for this study, we re-categorized the 59 classes into six major types (Types 1–6; see Table I) in the same manner as Suzuki *et al.* (2000) (see Plate 1 for its distribution). The re-categorized type occurring most frequently in the $1° \times 1°$ box (6×6 pixels) that included a GDS station near the centre of the box was adopted as the land cover for the GDS station.

2.4. Snow cover area map

The snow cover area indicated in Plate 2 is based on the 'weekly digital northern hemisphere snow and ice product', a satellite-derived snow cover map compiled by the NOAA National Environmental Satellite, Data and Information Service (NESDIS). This dataset contains information on the presence or absence of snow cover in each of 89×89-grid boxes on a polar stereographic map that covers most of the Northern Hemisphere (Masuda *et al.*, 1993). These weekly data were edited to 5-year (1987–1991) monthly composites. First, any weekly composite that had 4 or more days in a month was assigned to that specific month and all weekly composites in the 5 years were assigned to their respective months. Any pixel having snow cover for more than 50% of a month was denoted as a snow-covered pixel for that month.

2.5. Cluster analysis of NDVI seasonal cycles

The NDVI seasonal cycle (i.e. the variation of the monthly NDVI from March through October) at each of the 611 GDS stations was classified using cluster analysis, a multivariate analysis for objective classification. For cases in which many objects exist (an object is a 'station' in our analysis), a matrix (square array) consisting of similarities, called amalgamated distances, between mutual objects was made. Types were found objectively (e.g. Everitt, 1980).

In this study, the amalgamated distance (similarity) D_{ab} between stations a and b was defined as:

$$D_{ab} = \sqrt{\sum_{m=3}^{10} (\mathrm{NDVI}_{am} - \mathrm{NDVI}_{bm})^2}. \tag{1}$$

NDVI_{am} is the 5-year monthly mean at station a in month m (March–October correspond to 3–10, respectively). NDVI_{bm} is the 5-year monthly mean NDVI at station b in month m. The definition of the distance is analogous to the geometric distance between two points on an Euclidean plane.

Table I. Re-categorization of the original 59 land-cover types into six major types is shown[a] (reproduced with permission from Suzuki *et al.*, 2000)

- Type 1 (tundra and polar desert): Tundra; wooded tundra margin or mountain scrub/meadow; polar desert
- Type 2 (taiga): Main boreal conifer forest; cold cropland and pasture; cold steppe/meadow; northern or maritime taiga
- Type 3 (snowy forest and mire): Snowy non-boreal conifer forest; conifer/deciduous forest; snowy deciduous forest; mires include peaty bogs and fens; snowy forest/field; southern dry taiga
- Type 4 (cool field): Cool farmland and settlements; cool grass/shrub; snowy field/woods complex
- Type 5 (warm grassland and steppe): Mild/warm/hot grass/shrub; semi-desert/desert scrub/succulent/sparse grass; cool/cold shrub semi-desert/steppe
- Type 6 (desert): Desert; warm/hot cropland irrigated extensively; sand desert

[a] Descriptions for the original classification by Olson (1992) were simplified.

1: Tundra & polar desert 2: Taiga 3: Snowy forest & mire

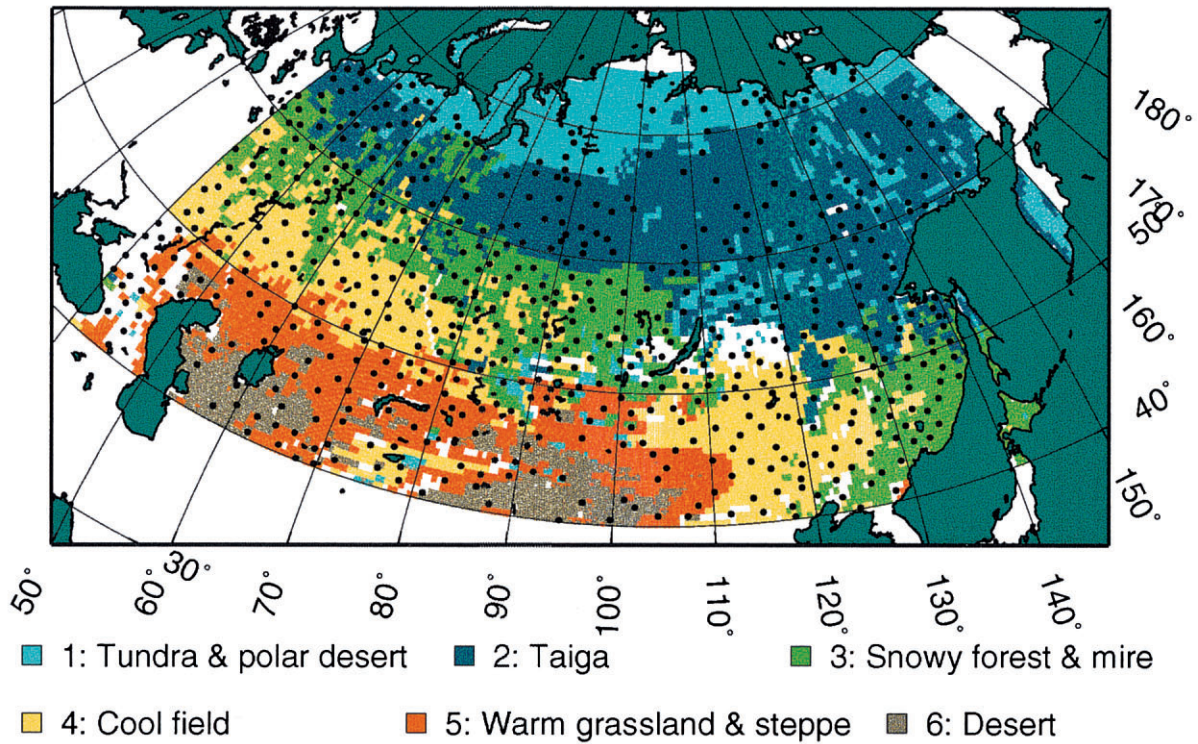4: Cool field 5: Warm grassland & steppe 6: Desert

Plate 1. The study region and the distribution of the six re-categorized land-cover types. White areas are not categorized. Details of each land-cover category are in Table I. The 611 GDS surface meteorological stations used in the analysis are indicated by dots (modified with permission from Suzuki *et al.*, 2000)
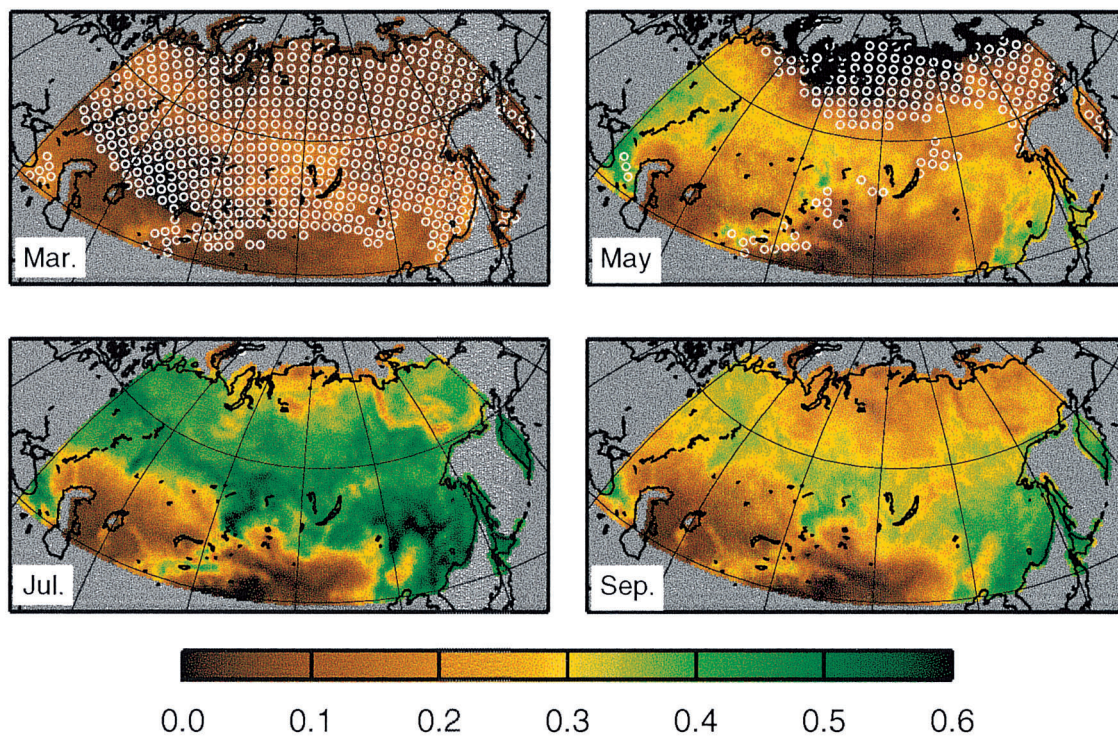

0.0   0.1   0.2   0.3   0.4   0.5   0.6

Plate 2. Monthly NDVI distribution in March, May, July and September. Mean snow cover area is denoted by small open circles
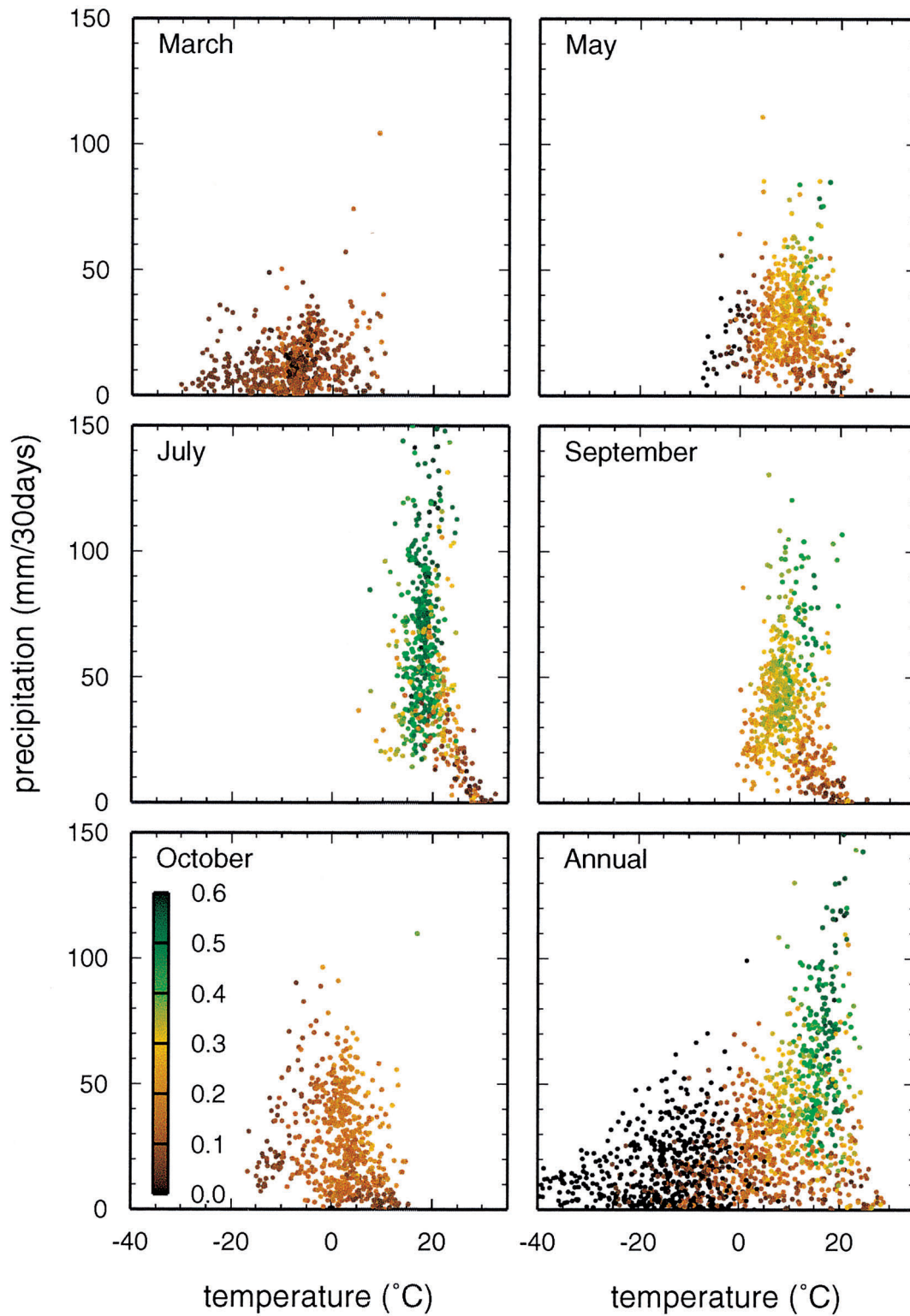
Plate 3. The relationship of NDVI, temperature and precipitation. For the monthly diagrams (March, May, July, September, October), values at all 611 GDS stations are plotted. For the annual diagram, values at 123 stations (about one-fifth of 611 stations) in all 12 months are plotted. Plotted circles are coloured by the NDVI value according to the colour scale shown. Plotted points that have no NDVI value (i.e. in November–February) in the annual diagram are black

In cluster analysis, a group of object(s) (i.e. station(s) in this analysis) is called a 'cluster.' In the D_{ab} matrix, the pair of clusters that have the smallest D_{ab} are combined as a newly established cluster. This process is repeated until there is a single cluster. This study combines clusters using the group average method, an agglomerative hierarchical technique that defines the distance between two clusters as the average of the amalgamated distances between all individual pairs in the two clusters (e.g. Everitt, 1980).

3. GENERAL FEATURES OF NDVI, LAND COVER, TEMPERATURE AND PRECIPITATION

3.1. Distribution of land-cover types

The six land-cover types in the study area are outlined in Plate 1. The land-cover types are zonally oriented; the west–east contrast is comparatively small. The vegetation in the southern part of the region (south of approximately 55°N) is dominated by non-forest vegetation, such as warm grassland and steppe (Type 5) and cool fields (Type 4). Desert (Type 6) is most prevalent around the Aral Sea and around 95°E/40°N. Snowy forest (mainly non-boreal) and mire (Type 3) are found to the north of the non-forest zone. Taiga (Type 2) is the dominant vegetation cover between 60 and 70°N. This taiga zone is wider in eastern Siberia than in western Siberia. The main land cover in the Arctic region, to the north of the taiga zone, is tundra and polar desert (Type 1). Type 1 is also located along some mountain ranges.

3.2. Seasonal variation of NDVI, temperature and precipitation distributions

Plate 2 shows the mean NDVI distribution in March, May, July and September. Areas of snow cover are denoted by small circles. In March, almost the entire region is snow covered, and the NDVI values are small. However, slightly larger NDVI (about 0.2) zone is noted along 60°N, especially in the western part from 110°E, and near Lake Baikal. This phenomenon is discussed in later section.

By May, the NDVI has markedly increased in 55–60°N, due to the greening-up of the vegetation, but the NDVI to the south and north is still low. Snow cover has diminished and is present only at latitudes poleward of 63°N. July is the peak month for the NDVI. High NDVI values cover Siberia; however, low NDVI values are maintained in arid regions (Types 5 and 6) around the Caspian and Aral Seas and in the Gobi desert. The NDVI is also relatively low for the region bordering the Arctic Ocean. Snow cover does not exist in July. In September, NDVI values are uniformly lower, due to the senescence of vegetation. The NDVI over arid regions in the southern part of the study area is persistently very low throughout the year.

Figure 1 shows the 5-year mean temperature distributions, derived from the 611 selected GDS stations, for March, May, July and September. The south–north temperature gradient found in every month highlights how the climate changes with latitude. In March, the lowest temperature (about $-25°C$) is over northeastern Siberia. Temperatures gradually increase to the south, eventually exceeding freezing in some parts along the southern boundary. In May, temperatures exceed freezing over most of the domain. July shows maximum temperatures at most stations (some in the southern region exceed 31°C) and a minimum north–south temperature gradient; the temperature difference between northern and southern regions is about 40°C in March, but only 10°C in July. The temperature drops over the entire region by September, when the temperature distribution is similar to that in May.

Figure 2 shows the 5-year mean precipitation distributions in March, May, July and September at the selected 611 GDS stations. In March and May, precipitation amounts and spatial gradients are small over the entire region. In July, however, a large regional contrast is present. Monsoonal activities along the southeast coast of the region generate much precipitation (more than 120 mm/30 days). In contrast, very little precipitation (less than 20 mm/30 days) falls in arid desert and steppe climates (Types 5 and 6) in the southwest. By September, precipitation is decreasing over the entire domain as summer ends.
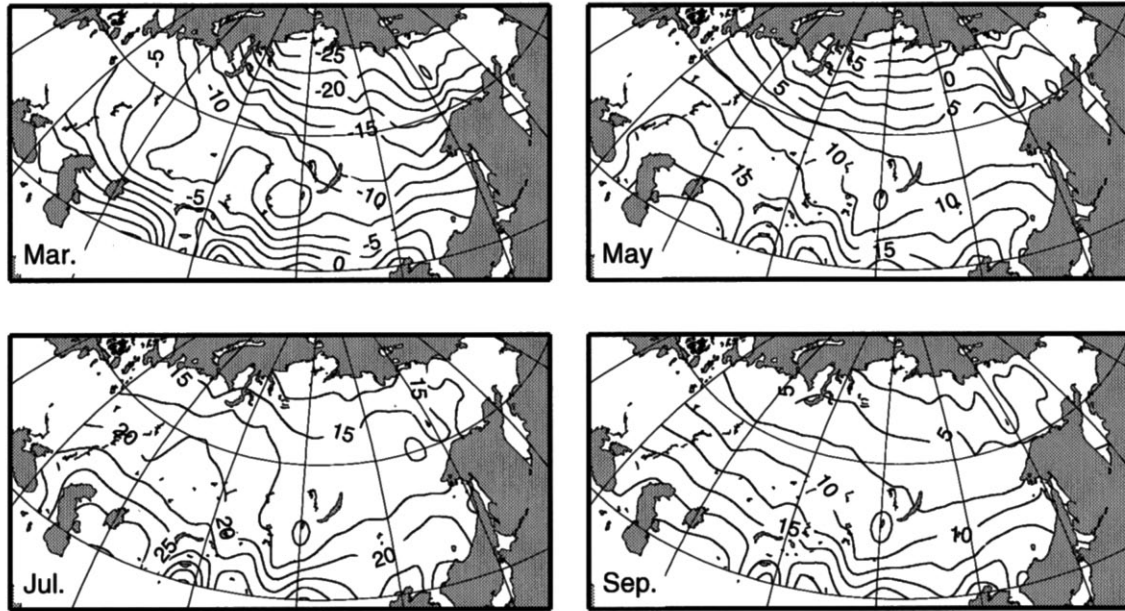
Figure 1. Monthly temperature in March, May, July and September (°C)

3.3. *Relationship among NDVI, temperature and precipitation*

This section focuses on the relationship between NDVI and climate, based on the analysis of the 611 selected GDS stations. Plate 3 shows the relationships between the NDVI, temperature, and precipitation. Each dot in the panel corresponds to a station value. In March, temperature, precipitation and the NDVI
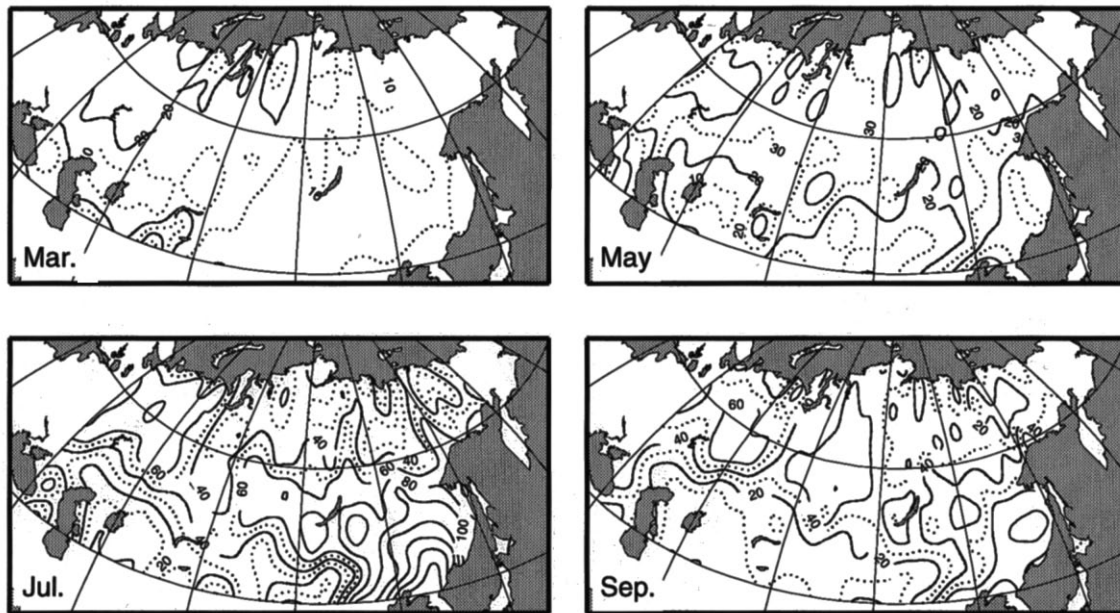

Figure 2. Monthly precipitation in March, May, July and September (mm/30 days). The solid contour interval is 20 mm/30 days. Dotted lines are drawn at 10, 30 and 50 mm/30 days

are all low, with no evident relationship. In May, the temperature and precipitation are greater than in March, and the NDVI also is greater, especially at stations with high temperatures and precipitation.

In July, the highest annual monthly temperature and precipitation occur. The temperature range becomes smaller (about 12–30°C), reflecting the quasi-uniform temperature distribution noted in Figure 1. In contrast, the range of precipitation is greatest, from 0–130 mm/30 days. The NDVI is generally high in July, however, the NDVI value is relatively low if the temperature exceeds 20°C and if precipitation is less than 20 mm/30 days. High temperatures and scant precipitation would reduce water available for vegetation, resulting in a low NDVI. This relationship between vegetation and temperature and precipitation is similar to the relationship between vegetation and a radiative dryness index, as shown by Budyko (1986).

The overall distribution in September resembles that in July, although the temperature and amount of precipitation are decreasing and the NDVI also decreases. These decreases in temperature, precipitation, and NDVI index continue in October, by which time the distribution is similar to that in May. After October, the three parameters decrease to winter minima, and then change to values seen in March.

Plate 3 also shows the annual relationship among the three parameters. The plotted points form a triangular area in the temperature and precipitation coordinate system. The diagram shows that a high NDVI occurs when the temperature is near 18°C and precipitation exceeds 20 mm/30 days. When temperatures exceed 20°C, the NDVI is comparatively small.

To examine the relationship between the maximum NDVI value and monthly temperature, a scatter diagram of these two parameters was constructed as shown in Figure 3. When precipitation is low (in the plot of 1–150 mm/year precipitation), no relationship is evident. However, for greater precipitation, there is a positive correlation between NDVI and temperature until the temperature reaches around 18°C ($r = 0.85$ for annual precipitation of 300–450 mm and temperature under 18°C). The NDVI decreases with increasing temperature for temperatures exceeding 18°C. The peak NDVI obviously occurs when the temperature is around 18°C, except when precipitation is low. This characteristic of the NDVI-temperature relation will be elaborated on in the discussion section.

4. CLASSIFIED SEASONAL CYCLES OF NDVI AND CLIMATE

4.1. Result of cluster analysis

Figure 4 shows a dendrogram indicating the linking processes among clusters. First, six clusters (A, B, C, D, E and F) were obtained at a distance of around 0.23. Clusters D and E were sub-classified, because many stations belonged to those two clusters (D: 136, E: 202). Cluster D was sub-classified into D1 and D2; Cluster E was broken into E1, E2, E3 and E4. Thus, ten clusters were obtained. These clusters henceforth will be termed 'Classes' to distinguish them from the 'Type' of land cover.
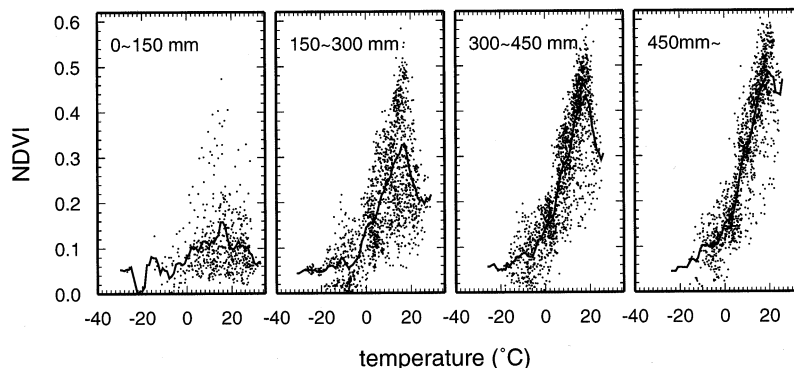

Figure 3. Relationship between the monthly NDVI and temperature at the 611 stations categorized by annual precipitation amount. The solid line denotes the smoothed variation
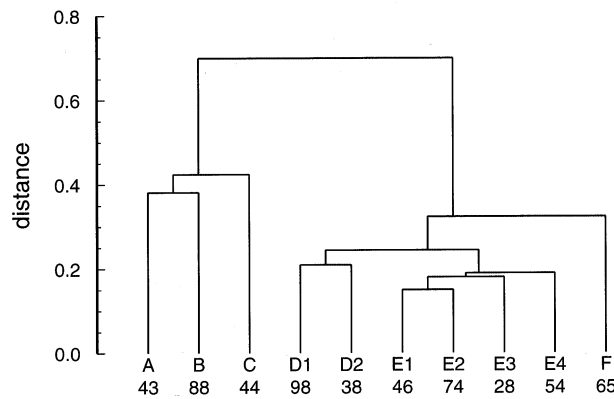
Figure 4. A dendrogram that indicates the process of categorization by cluster analysis. The number below each class name is the number of stations belonging to each class

In addition to these ten clusters, the classification process produced three minor clusters, which include 20, 8 and 5 stations and are not indicated in Figure 4. These three clusters were not designated as 'Classes', because of the small number of stations in each. Subsequently, 33 of the 611 stations (5.4%) were excluded from the classification. Figure 5 shows the geographical distribution of the 10 classes.

4.2. Outline of the seasonal cycles

Figure 6 presents the averaged monthly values of NDVI, temperature and precipitation for each class. Except for Class C, the NDVI shows an obvious unimodal seasonal cycle. The NDVI in March and April is generally small, then abruptly increases in May or June. The NDVI peaks around July, then subsequently decreases as winter approaches. The seasonal characteristics of the NDVI delineate the vegetation phenology over the study area: the dormancy of vegetation from winter to spring, the greening-up phase due to the snow thawing and foliation in May or June, the greenest month around July, and senescence to dormancy phases in autumn–winter seasons.

Temperature and precipitation also show an unimodal seasonal cycle (except for the precipitation for Class C). The maximum temperature and precipitation occur in the summer season, overlapping the maximum in the NDVI. These similar seasonal cycles among the NDVI, temperature and precipitation underline the importance of climatic factors in controlling vegetation phenology.
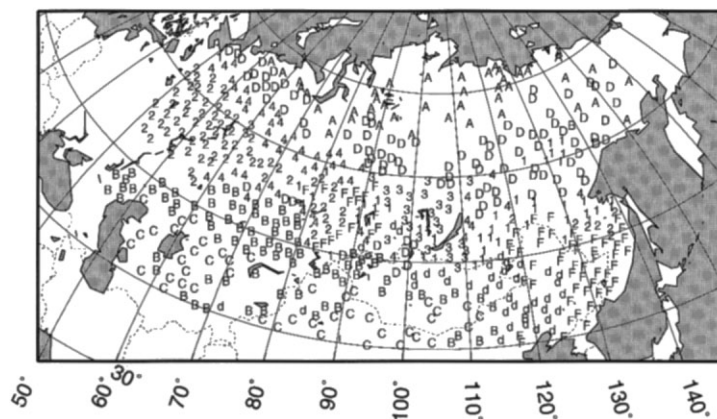

Figure 5. Geographical distribution of the NDVI seasonal cycle classes as classified by cluster analysis. Classes D1 and D2 are denoted by 'D' and 'd', respectively. Classes E1–E4 are indicated by '1'–'4', respectively
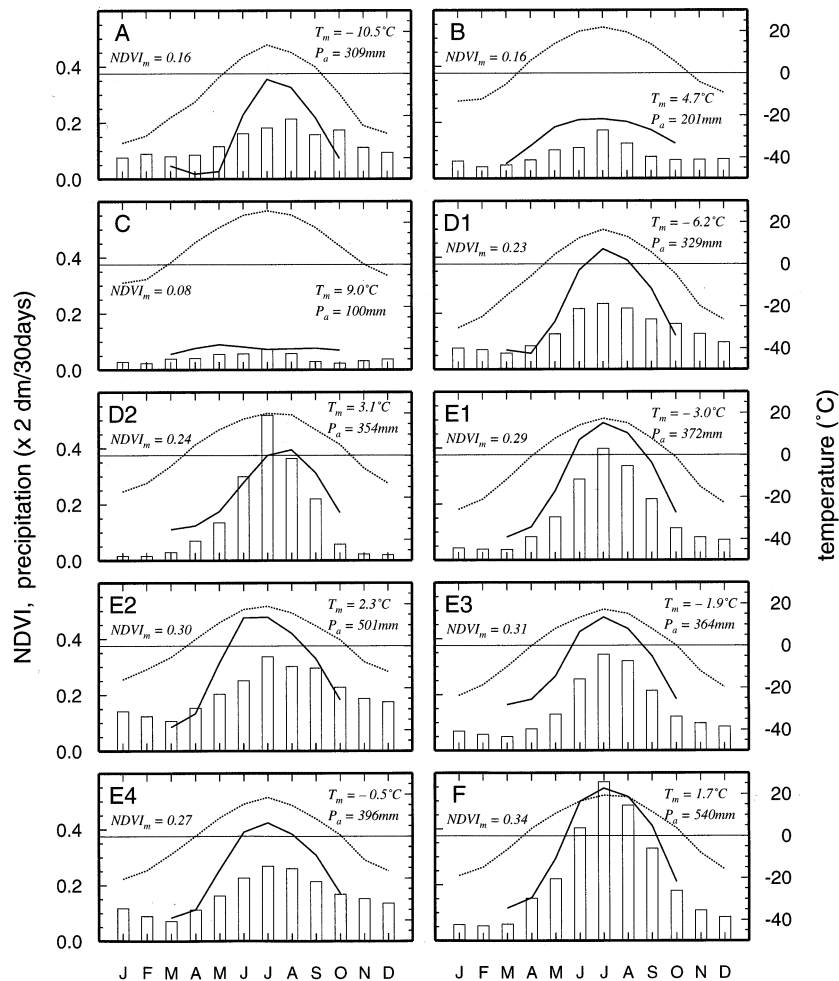
Figure 6. The seasonal change in the monthly mean NDVI (solid line), temperature (dotted line) and precipitation (bar) for each cluster. The unit of the precipitation ordinate is not simple due to the relation to the NDVI ordinate. For example, '0.4' on the precipitation ordinate equals 80 mm/30 days. $NDVI_m$, T_m and P_a in each panel are the annual mean NDVI, annual mean temperature and annual precipitation, respectively

We analysed the relationship between the NDVI seasonal cycle class and the modified (re-categorized) Olson's land-cover types shown. Figure 7 presents the proportional ratios of land-cover types for each NDVI Class. Although each class does not always correspond to a sole land-cover type, each class is featured by a particular land-cover type. Based on the ratio of the land-cover type, Classes A–F are categorized as follows: (1) Class A—tundra and polar desert (Type 1); (2) Classes D1, E1, and E4—taiga (Type 2); (3) Classes E2, E3, F—snowy forest and mire (Type 3); (4) Class D2—cool field (Type 4); and (5) Classes B and C—arid type land covers (Types 5 and 6). From Figures 5–7, the detailed features of each class can be described in five groups as follows.

4.3. Class characteristics

4.3.1. Class A (43 stations). Stations in Class A cover the northern part of the study area, near the Arctic Ocean, and are dominated (60%) by tundra and polar deserts (Type 1). The NDVI shows an obvious seasonal cycle with small amplitude. The abrupt increase in the NDVI that takes place in June lags 1 month behind other classes (except Class C). The maximum value of NDVI in Class A in July is
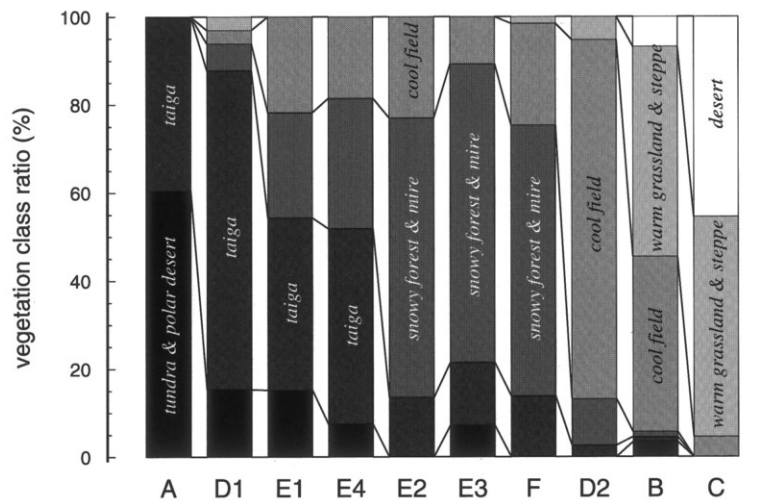
Figure 7. The ratio of land-cover type in each NDVI seasonal cycle class

0.36, the third lowest July value after Classes C and B. The annual mean temperature in Class A (-10.5°C) is the lowest of the classes. Total precipitation is small (309 mm/year), and the amplitude of the seasonal cycle is small.

4.3.2. Classes D1 (98 stations), E1 (46 stations) and E4 (54 stations). Class D1 is adjacent and south of Class A. Class E1 is mainly south of D1, over southeastern regions of Russia. Class E4 extends between Classes D1 and E2. These three classes (D1, E1 and E4) roughly correspond to taiga (Type 2), as seen from Plate 1 and Figure 7.

The NDVI of these three classes in spring is around 0.1; it subsequently increases from spring to summer. The maximum NDVI occurs in July and exceeds 0.4. The NDVI seasonal amplitude is larger than in Classes A, B and C. The annual mean temperature ranges from -6.2 to -0.5°C, which is low compared with other classes (except for Class A). Annual precipitation is 329–396 mm.

The NDVI seasonal cycles among these three classes are similar, although class-to-class differences exist as follows. Class D1 is characterized by lower NDVI than Classes E1 and E4, especially in April and May. The spring greening-up in Class D1 is delayed by the lower temperature in that region compared with the other two classes. Class E1 is remarkable for the high NDVI (0.49) in July, a value exceeded only in Class F. The seasonal cycles of temperature and precipitation for Class E4 are midway between those of Classes D1 and E2.

4.3.3. Classes E2 (74 stations), E3 (28 stations) and F (65 stations). The dominant land-cover types for these three classes are snowy forest and mire (Type 3). These three classes are south of Classes D1, E1 and E4, and temperatures are generally higher than in Classes D1, E1 and E4.

Class E2 is over the western part of the domain, between 50° and 60°N. A notable feature here is the early occurrence of a large NDVI in June, which nearly equals July values. This suggests that the greening-up season occurs earlier in Class E2 than elsewhere. Suzuki *et al.* (1997) analysed this regional feature of the NDVI seasonal cycle and suggested that it was related to relatively high precipitation and winter temperatures. The outstanding feature of Class E3, which is found in the central region around Lake Baikal, is that it has the largest values of NDVI in March and April (discussed in the later section). The seasonal cycles of temperature and precipitation are similar to those of Class E1.

The annual mean NDVI for Class F is the highest (0.34) of all the classes. The seasonal cycle of NDVI for Class F is characterized by its large amplitude. The NDVI in September is the highest (0.41) for all the classes, reflecting the late onset of the decrease in autumn. Precipitation in Class F is the highest (540 mm/year) of all classes and is the result of monsoon activity in the summer. This class is found in the

southeastern part of the study area, near the Sea of Japan. It is northeast of Class D2. Some Class F stations also exist near 90°E between 50° and 60°N, a region far from the Sea of Japan. The forest vegetation in these two geographically distant regions has similar phenological characteristics, i.e. a high maximum NDVI and a delayed decrease in autumn. Both regions are characterized by large amounts of precipitation.

4.3.4. Class D2 (38 stations). Class D2 consists mostly (82%) of cool fields (Type 4), and extends from near the southern part of Lake Baikal to northeast China though Mongolia, to the north of Class B. The NDVI of Class D2 in spring is relatively large (0.12) compared with Class D1. Class D2 reaches a maximum NDVI (0.39) in August. The mean annual temperature is 3.1°C, which is relatively high, as in Class B. Precipitation falls mostly in the summer and totals 354 mm/year. It appears that the relatively dry climate is not suitable for forest vegetation.

4.3.5. Classes B (88 stations) and C (44 stations). Classes B and C are characterized primarily by arid land cover, such as grassland, steppe (Type 5) and desert (Type 6). The amplitude of the NDVI seasonal cycle of Class B is small, and the maximum NDVI is also small (0.21 in July). The NDVI in Class C has almost no seasonal variation, with consistently low values (< 0.1) throughout the year. The annual maximum NDVI is 0.09 in May.

The annual precipitation for Class C is the lowest (100 mm/year) for all classes and that of Class B is the second lowest (201 mm/year). The mean annual temperature of Class C is the highest (9.0°C) of all the classes. The mean temperature in July reaches 25.7°C. Little precipitation and high temperatures in Classes B and C restrict the water available for vegetation, thus causing the low NDVI throughout the year. Especially for Class C, no response of green vegetation is discerned in the NDVI seasonal cycle.

Class C stations are found mostly in the southern part of the study region, around the Caspian and Aral Seas, in southern Mongolia and in northern China. The Class C region is bordered to the north by Class B. These two classes cover a wide area latitudinally, especially west of 90°E. In the east, they are more restricted to the southernmost part of the domain. This east–west difference in the distribution seems to be related to the topography.

The analyses in this section highlighted the spatial distribution of the NDVI seasonal cycle and how it is related to temperature, precipitation, and land-cover type. Classes A–F are regionally distinct. In other words, no region has significant areas of mixed classes. This suggests that each local region contains vegetation with a distinct phenological cycle. Climate is the main factor controlling the distribution of the classes, but topography, soil type and the existence of permafrost are also important.

5. DISCUSSIONS

5.1. A high NDVI zone emerged around 60°N in March

Plate 2 shows the NDVI distribution in March. There are slightly elevated NDVI values (0.1–0.2) in a west-east zone around 60°N, despite the existence of snow cover. This large NDVI zone is apparent in the west of 110°E and near Lake Baikal. As expected, the NDVI seasonal cycle of Classes E3, E2, and F, which cover this region, shows NDVI values in March and April that are relatively larger than those of other classes.

These classes are dominated by Type 3 (snowy forest and mire). Although Olson's vegetation map does not provide sufficient information of forest distribution in Siberia with regard to deciduous or non-deciduous, Type 2 includes non-deciduous forest vegetation that should have green leaves on its canopy even in winter.

Vegetation maps (e.g. Principal Administration of Geodesy and Cartography, 1984) show that the primary vegetation in the forest zone west of the Yenisey River and in the mountainous regions near Lake Baikal is non-deciduous forests (e.g. fir and spruce). In eastern Siberia, the primary vegetation is the deciduous larch tree. It is considered that this non-deciduous/deciduous regionality of forest vegetation

may be observed by satellite remote sensing, as the high NDVI in March. Although the forest floor is covered by snow and the region was judged as a 'snow covered area' by the satellite remote sensing as indicated in Plate 2, the forest green canopy above the snow cover may contribute to the formation of the relatively large NDVI zone in March.

5.2. *Peak NDVI where monthly temperatures are around 18°C*

As shown in Section 3, the NDVI reaches a maximum when the monthly mean temperature is around 18°C. This section discusses the climatological significance of the 18°C temperature threshold on vegetation in Siberia.

Figure 8 is a detailed enhancement of the NDVI-temperature relationship in Figure 3 for June, July and August. These months were selected because the NDVI reaches its maximum value at almost all stations during this period. Plotting symbols (A–F) are the NDVI seasonal cycle class determined by the cluster analysis. The highest NDVI (0.59) occurs in July for monthly temperatures around 18°C. The NDVI maxima are somewhat smaller in June and August. Furthermore, the maximum peak in these months is less striking than in July. Moreover, NDVI values in June and August are uniformly smaller than those in July, suggesting that the maximum NDVI peak around 18°C occurs in July.

Classes F, E and D1 are the dominant classes in the NDVI maximum peak in July. These are all forest classes. The NDVI of them in summer exceeds 0.4; the maximum monthly temperature is around 18°C; and there is adequate precipitation. If the monthly temperature is less than 18°C, the dominant NDVI seasonal cycle class is Class A, which has a smaller maximum NDVI. Class A is associated with tundra. If the temperature is greater than 18°C, the main classes are Classes B and C, which are characterized by a low NDVI, high temperature and low precipitation. These are arid classes.

Thus, stations with a July monthly temperature of around 18°C are likely to contain the greenest (and perhaps thickest) vegetation. If the temperature is less than 18°C, the greenness of the vegetation is inhibited by low temperatures. If the temperature is greater than 18°C, greenness is inhibited by aridity.

The regions where the annual maximum monthly NDVI exceeds 0.45, and the stations that have annual maximum monthly temperatures between 16.5 and 19.5°C (i.e. around 18°C) are shown in Figure 9. The figure shows that the high NDVI is zonally distributed, mainly between 50° and 60°N; in this zone, the maximum temperature is around 18°C. Although the two zones do not perfectly overlap (especially around 70°E and in the southeast part of the domain), good overall agreement exists. North of this 18°C zone, the temperature drops uniformly towards the pole to less than 16.5°C. South of the 18°C zone, the temperature exceeds 19.5°C, except for mountainous regions near the Russia–Mongolia border.
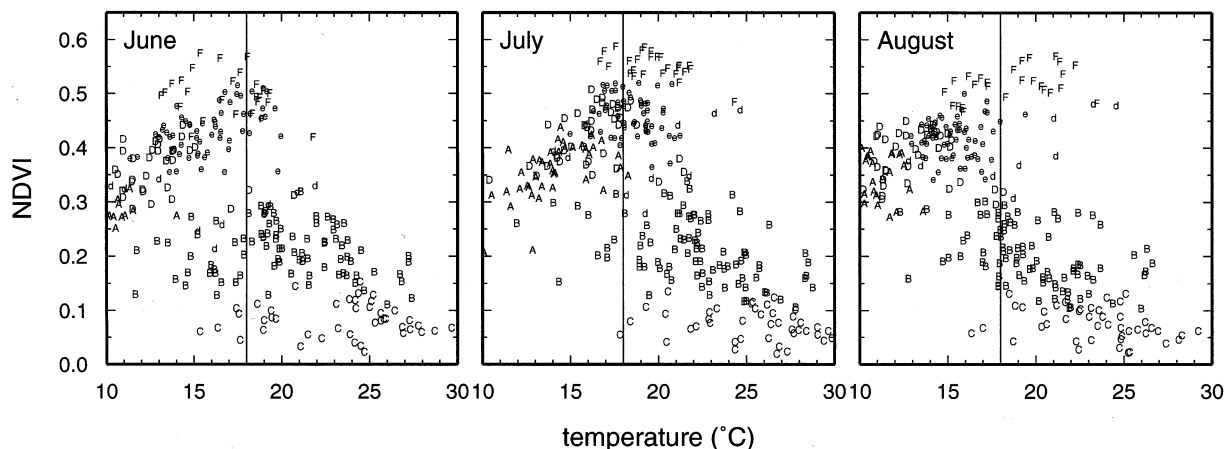

Figure 8. The relationship between monthly NDVI and temperature in June–August. Points are plotted using the symbol for the NDVI seasonal cycle class. Classes D1 and D2 are denoted by 'D', and 'd', respectively. Classes E1–E4 are all denoted by 'e'. For Classes D1, D2, E1–E4 and F, data are plotted for one-third of the stations, which were selected arbitrarily, for reasons of clarity. A vertical line is drawn at 18°C for convenience
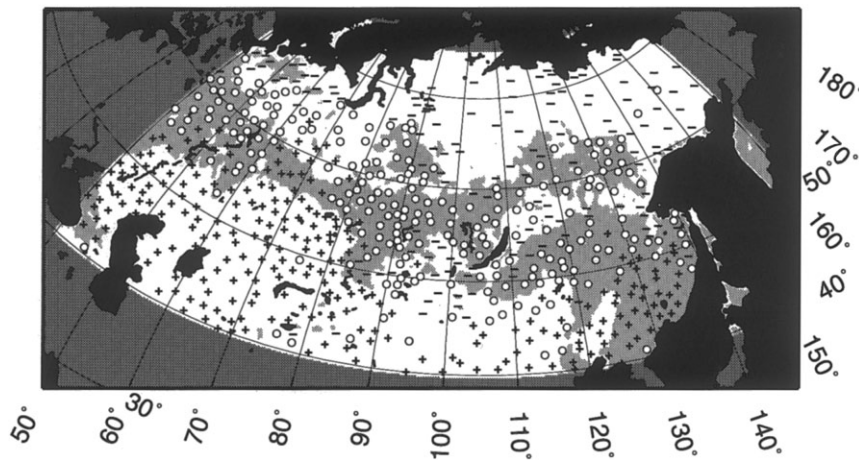
Figure 9. The region with the annual maximum monthly NDVI over 0.45 (hatched area) and the GDS station with the annual maximum monthly temperature between 16.5 and 19.5°C (open circle). The stations with temperatures greater than 19.5°C or less than 16.5°C are denoted by ' + ' and ' − ', respectively

It can be considered that the zone where the maximum temperature is around 18°C has climatologically the greatest potential for a high NDVI, and the NDVI in the north region from that zone is diminished by low temperature, while the NDVI in the southern region from that zone is diminished by aridity in the study region. This result is consistent with Suzuki *et al*. (2000) who revealed the gradient in NDVI from forest to tundra is dominated by temperature, and that from forest to steppe/desert is dominated by aridity in two north–south transects in Siberia.

It is not clear why the maximum NDVI occurs at 18°C in the study area. An optimal temperature–precipitation relationship for the vegetation may form coincidentally in the geographical zone where the maximum monthly temperature is around 18°C. To understand more fully the significance of the 18°C value, a study of the NDVI-climate relationship in other regions of the world is necessary. Alternatively, a more detailed investigation of our study region, to identify local regional conditions more precisely, could be made.

For example, a slightly different relationship between NDVI and temperature is evident in the southeast portion of our study region, where Class F dominates. In this region, the high NDVI values correspond to temperatures higher than 18°C, as indicated in Figure 9. Precipitation in this region is much greater than in other regions (Figure 2). This enhanced precipitation may support a sufficiently humid climate for the local vegetation, in spite of temperatures greater than 18°C. Thus, it is possible that the optimum temperature, which is around 18°C in Siberia, changes with global climatic zone. In addition, the possibility that this temperature shifts with the statistical period of the analysis cannot be ignored.

6. CONCLUSIONS

The NDVI seasonal cycle and its spatial distribution were investigated and related to temperature and precipitation in the region bounded by 40° and 160°E, and 40° and 75°N. This region includes Siberia primarily. The analysis was carried out using 5-year (1987–1991) monthly means. Monthly temperatures and precipitation were calculated at 611 surface stations in the study region using daily data from the GDS CD-ROM. The NDVI was obtained from the third-generation monthly global NDVI product, and 5-year monthly mean NDVI values at the 611 GDS stations were calculated.

The 611 stations were classified by cluster analysis based on the seasonal cycle (March–October) of the NDVI, and ten classes were obtained. The characteristics of each class were described in conjunction with temperature, precipitation and Olson's land-cover type, and consequently the regional characteristics of the NDVI seasonal cycle were revealed. Class A covered the region near the Arctic Ocean, where tundra

vegetation prevails; its NDVI seasonal cycle has a small amplitude and a 1-month delay in greening-up compared with other classes. In the southern arid regions, where temperatures are high and precipitation scant, the seasonal fluctuation in the annual NDVI march is hard to see (Class C) or relatively small (Class B). Major forested regions were categorized into six classes (Classes D1, E1–4 and F), and all of these classes show large amplitude in the NDVI seasonal cycle, especially the non-boreal forest classes. Furthermore, these six forest classes show characteristics related to the land-cover type in addition to the seasonal temperature and precipitation cycles.

A region that shows a relatively large NDVI value in March, even when snow covered, was investigated. The high NDVI value may be related to the exposed green canopy of the non-deciduous forest in the snow-covered area. NDVI is maximized in regions where the maximum monthly temperature is around 18°C, suggesting that the optimum temperature–precipitation environment for vegetation is found where the maximum monthly temperature is 18°C.

These results improve our knowledge of the climate and of the phenology and distribution of vegetation in Siberia. Moreover, the results aid our understanding of the impact of vegetation on the climate system over an extensive region of the globe. In the future, the results of this paper will be compared with surveys of other terrestrial areas to evaluate other vegetation–climate relationships. Topography, soil type and permafrost can also influence the Siberian vegetation. Their relationships could be the target of a future study using NDVI.

ACKNOWLEDGEMENTS

REFERENCES

Budyko MI. 1986. *The Evolution of the Biosphere*. D. Reidel: Holland. Translated by MI Budyko, SF Lemeshko, VG Yanuta.
DeFries RS, Townshend JRG. 1994. NDVI-derived land cover classifications at a global scale. *International Journal of Remote Sensing* **15**: 3567–3586.
Everitt B. 1980. *Cluster Analysis* (2nd edn). Halsted Press: New York.
GAME–International Science Panel. 1998. *GEWEX Asian Monsoon Experiment (GAME) Implementation Plan*.
Goward SN, Ye DG, Turner S, Yang J. 1993. Objective assessment of the NOAA global vegetation index data product. *International Journal of Remote Sensing* **14**: 3365–3394.
Gutman G. 1999. On the use of long-term global data of land reflectance's and vegetation indices derived from the advanced very high resolution radiometer. *Journal of Geophysical Research* **104**: 6241–6255.
Gutman G, Tarpley D, Ignatov A, Olson S. 1995. The enhanced NOAA global land dataset from the advanced very high resolution radiometer. *Bulletin of the American Meteorological Society* **76**: 1141–1156.
IPCC. 1996. Climate change 1995: the science of climate change. Contribution of working group I to the second assessment report of the Intergovernmental Panel on Climate Change, Cambridge University Press, Cambridge, UK.
Justice CO, Townshend JRG, Holben BN, Tucker CJ. 1985. Analysis of the phenology of global vegetation using meteorological satellite data. *International Journal of Remote Sensing* **6**: 1271–1318.
Kidwell KB. 1997. *NOAA Global Vegetation Index User's Guide*. US Department of Commerce, NOAA, NESDIS, NCDC, http://www2.ncdc.noaa.gov/docs/gving/cover.htm. Accessed 2000.
Masuda K, Morinaga Y, Numaguti A, Abe-Ouchi A. 1993. The annual cycle of snow cover extent over the northern hemisphere as revealed by NOAA/NESDIS satellite data. *Geographical Reports of Tokyo Metropolitan University* **28**: 113–132.
Moulin S, Kergoat L, Viovy N, Dedieu G. 1997. Global-scale assessment of vegetation phenology using NOAA/AVHRR satellite measurements. *Journal of Climate* **10**: 1154–1170.
Myneni RB, Keeling CD, Tucker CJ, Asrar G, Nemani RR. 1997. Increased plant growth in the northern high latitudes from 1981 to 1991. *Nature* **386**: 698–701.
Myneni RB, Tucker CJ, Asrar G, Keeling CD. 1998. Interannual variations in satellite-sensed vegetation index data from 1981 to 1991. *Journal of Geophysical Research* **103**: 6145–6160.
NOAA National Climate Data Center. 1994. Global Daily Summary (CD-ROM).
NOAA National Climate Data Center. 1998. Time Series of Global Monthly Vegetation Cover from NOAA/AVHRR: April 1985–December 1997 version 1. Published on CD-ROM by NOAA/NESDIS/NCDC.
Norwine J, Greegor DH. 1983. Vegetation classification based on Advanced Very High Resolution Radiometer (AVHRR) satellite imagery. *Remote Sensing and Environment* **13**: 69–87.
Olson JS. 1992. World Ecosystems (WE1.4), Digital Raster Data on a 10-minute Geographic 1080 × 2160 grid. In *Global Ecosystems Database*, *Version 1.0: Disc A*. National Geophysical Data Center (CD-ROM).

Principal Administration of Geodesy and Cartography. 1984. *Atlas S.S.S.R, Soviet Union*. USSR Government.

Rao CRN, Chen J. 1995. Inter-satellite calibration linkages for the visible and near-infrared channels of the Advanced Very High Resolution Radiometer on the NOAA-7, -9, and -11 spacecraft. *International Journal of Remote Sensing* **16**: 1931–1942.

Rao CRN, Chen J. 1996. Post-launch calibration of the visible and near-infrared channels of the Advanced Very High Resolution Radiometer on the NOAA-14 spacecraft. *International Journal of Remote Sensing* **17**: 2743–2747.

Suzuki R, Yatagai A, Yasunari T. 1997. Vegetation index and evapotranspiration in Siberia. In *Research Report of IHAS (Proceedings of International Workshop on Energy and Water Cycle in GAME-Siberia)*, Fukushima Y, Ohata T (eds). Nagoya University **3**: 84–93.

Suzuki R, Yatagai A, Yasunari T. 1998. Satellite-derived vegetation index and evapotranspiration estimated by using assimilated atmospheric data over Asia. *Journal of the Meteorological Society of Japan* **76**: 663–671.

Suzuki R, Tanaka S, Yasunari T. 2000. Relationships between meridional profiles of satellite-derived vegetation index (NDVI) and climate over Siberia. *International Journal of Climatology* **20**: 955–967.

Tarpley JD. 1991. The NOAA global vegetation index product—A review. *Palaeogeography*, *Palaeoclimatology*, *Palaeoecology (Global Planetary Change Section)* **90**: 189–194.

Tarpley JD, Schneider SR, Money RL. 1984. Global vegetation indices from the NOAA-7 meteorological satellite. *Journal of Climate and Applied Meteorology* **23**: 491–494.

Walter H. 1973. *Vegetation of the Earth—In Relation to Climate and the Eco-physiological Condition*. Springer-Verlag: New York. Translated by J Wieser.

Wessel P, Smith WHF. 1991. Free software helps map and display data. *EOS Transactions*, *American Geophysical Union* **72**: 441–445, 446.

Woodward FI. 1987. *Climate & Plant Distribution*. Cambridge University Press: Cambridge.

Ye H, Cho H-R, Gustafson PE. 1998. The change in Russian winter snow accumulation during 1936–83 and its spatial patterns. *Journal of Climate* **11**: 856–863.